On the use of different variance reduction techniques within MCNP to calculate the flux on the concrete walls of a pressurized water reactor

Mariya Brovchenko, Léa Tillard, Kenneth William Burn, Bertrand Cochet, A. Jinaphanh

ON THE USE OF DIFFERENT VARIANCE REDUCTION TECHNIQUES WITHIN MCNP TO CALCULATE THE FLUX ON THE CONCRETE WALLS OF A PRESSURIZED WATER REACTOR

Mariya Brovchenko[1], **Léa Tillard**[1], **Kenneth W. Burn**[2], **Bertrand Cochet**[1 *], **Alexis Jinaphanh**[1 †]
[1]Institut de Radioprotection et de Sûreté Nucléaire
31 avenue de la Division Leclerc 92260 Fontenay-aux-Roses CEDEX France

[2]ENEA
Via M.M.Sole, 4, 40129 Bologna, Italy

mariya.brovchenko@irsn.fr, lea.tillard@irsn.fr, kenneth.burn@enea.it

ABSTRACT

Monte-Carlo particle transport codes are commonly used as reference calculation schemes to simulate large systems such as Pressurized Water Reactors (PWR). In particular, the calculation of ex-core flux-related quantities often requires the use of variance reduction techniques, which themselves rely on pre-calculated importance maps. This work proposes a comparison of the performances associated with the use of different weight maps produced by methods based either on Monte-Carlo codes or on deterministic codes, applied to detectors placed in the concrete wall of a PWR. Also, the data published in this paper are public and open data, so that interested researchers can use these published results for benchmark purposes.

KEYWORDS: variance reduction, benchmark, reactor shielding

1. INTRODUCTION

Many countries are facing either the lifetime extension or the dismantling of their nuclear power reactors. For both issues an evaluation of the radiation environment outside the reactor vessel is needed. Monte-Carlo allows to model complex geometries using continuous energy cross sections. However to evaluate with a reasonable variance a quantity of interest far from the neutron source requires long computational time. To circumvent this problem, variance reduction methods can be used. Among existing variance reduction methods some require a greater experience in their use than others. Wrongly constructed variance reduction parameters may lead to an underestimation of the score if an important contributor is missed by the method. Caution must be taken in choosing which variance reduction method to use. In this paper, the authors have chosen to focus on the use of the Weight Window method implemented in MCNP [1] that allows to control the track weight in phase space using the splitting and the Russian Roulette methods. The basic idea is to vary

*Work performed while at IRSN, now at CEA, current address: bertrand.cochet@cea.fr
†Work performed while at IRSN, now at CEA, current address: alexis.jinaphanh@cea.fr

the track population through a definition of the expected track weight in each segment of phase space and at the same time to limit the weight dispersion in the case that some other variance reduction technique is simultaneously employed. The challenge is then to specify the weights for each segment of phase space. To do so, several approaches are proposed, based on Monte Carlo or deterministic methods. The originality of this work is that it tries to compare a larger spectrum of methods on a benchmark which presents several difficulties, such as a strong variation of the importance within the source region and the detector positioning at different azimuthal angles. The benchmark is described in detail in this paper, in order to give the possibility to others to contribute to this comparison exercise.
The CADIS (Consistent adjoint driven importance sampling) [2] methodology seems very interesting, but since it is based on a deterministic calculation it may have certain congenital disadvantages such as the multi-group treatment of nuclear data or spatial and directional discretization precision. Among this type of methods, the authors have tested the ADVANTG [3] and ATTILA [4] tools. Monte-Carlo based methods do not have these disadvantages, but need more computational time and sometimes more user experience to construct the variance reduction parameters. The Weight Window Generator (WWG) [5] and DSA [6] methods were tested here. All these methods were used to create a weight map over phase space used to accelerate the MCNP calculation using the weight window method. WWG, ATTILA and ADVANTG are based on the estimation of the importance function or the adjoint flux, while the DSA method estimates the best parameters to maximize the figure of merit, taking into account the variance and the calculational time of the contributors. Other authors suggest in [7] that the adjoint flux is not necessarily the optimal solution especially for neutron-photon problems, where the calculational times of neutron and photon histories are not comparable. In order to be aware of the advantages and limits of the various approaches, the authors have tested some of them on a computational benchmark. The choice of the benchmark was motivated by the need of dosimetry and activation evaluations outside the vessel.

2. Benchmark description

The reactor model is based on the start-up data of the Tihange-I reactor (PWR), producing a nominal electric power of 900 MW. Following the first divergence of the core in 1975, start-up physics tests were performed and described in [8]. The studied Tihange-I core is freshly fueled with three different ^{235}U mass enrichments 1.95% (fuel density $6.83546 \cdot 10^{-2}$ at/bn/cm), 2.55% ($6.83565 \cdot 10^{-2}$ at/bn/cm) and 3.10% ($6.835818 \cdot 10^{-2}$ at/bn/cm), no burnup, and at hot zero power state (no thermal hydraulics feedback). The reactor model outside the core is based on approximate data of a French PWR, already used in previous studies by the authors [9].

2.1. Model

The assembly is composed of 15x15 (225) rods. All assemblies have 204 fuel rods and 21 guide tubes. Some assemblies contain 8 or 12 poisoned rods inserted in the guide tubes, as shown in Figures 1a and 1b. Some assemblies may also contain an instrumentation tube that is positioned inside the guide tube of the central rod as shown in Figure 1b. Some guide tubes contain no structure and are modeled with borated water inside (dark blue in Figure 1).
All the dimensions of the rods are given in Table 1 and the compositions and densities, as defined in the MCNP input, are detailed in APPENDIX A. This appendix gives also the densities and the compositions of all other materials in the benchmark except the fresh fuel which is defined in

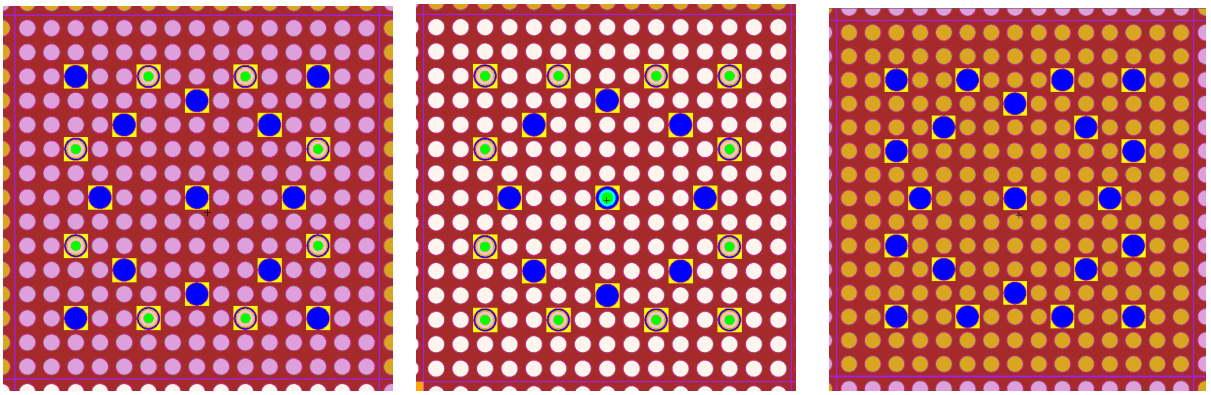

(a) Fuel rods (magenta), 8 rods with poison and 13 empty guide tubes

(b) Fuel rods (white), 12 rods with poison, 8 empty guide tubes and 1 instrumentation tube in the center

(c) Fuel rods (orange) and 21 guide tubes

FIGURE 1: Horizontal section of the MCNP models of 15x15 assembly : 3 configurations of 0, 8 or 12 rods with neutronic poison (coral), guide tube in the center may contain an instrumentation tube (blue), other guide tubes contain only water (dark blue).

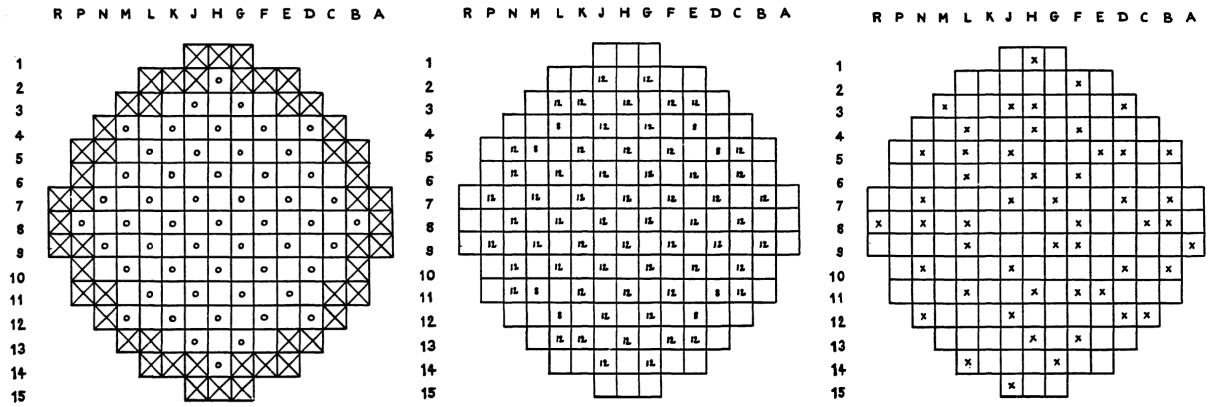

(a) Uranium enrichment in ^{235}U of the assemblies

(b) Poisoned rods positions : 8 and 12

(c) Positions of instrumentation tubes

FIGURE 2: Positioning in the core of the assemblies with different enrichment, poisoned rods and instrumentation tubes [8].

section 2. The cladding of the fuel rods and guide tubes is made of Zircaloy. The fuel rod contains helium between the fuel and the cladding. The poison rod is composed of an inner and an outer cladding made of SS 304. In between the two claddings is located the poison surrounded on both sides by helium. Inside the inner cladding helium is also present (light green in Figure 1). The instrumentation tube is modeled as a SS 316 tube filled with helium. The instrumentation tube and

the rod with neutronic poison are surrounded by water and a guide tube. Water located between the fuel rods and guide tubes is a mixture of borated water and steel since it takes into account the presence of fuel assembly structures. The core is composed of 3 enrichment zones presented in Figure 2a. The positions of the instrumentation tubes are shown in Figure 2c and the number of poisoned rods in the assembly is given in Figure 2b.

TABLE 1: Geometry of the model

Fuel pin radius	0.465793 cm
Clad inner radius	0.474956 cm
Clad outer radius	0.53677 cm
Guide tube inner radius	0.651252 cm
Guide tube outer radius	0.694499 cm
Burnable poison inner cladding inner radius	0.2851718 cm
Inner cladding outer radius	0.301759 cm
Poison inner radius	0.31115 cm
Poison outer radius	0.49784 cm
Outer cladding inner radius	0.5110126 cm
Outer cladding outer radius	0.580136 cm
Instrumentation tube inner radius	0.33813 cm
Outer radius	0.491245 cm
Fuel height	365.8 cm
Fuel pin lattice	1.435 cm

Assembly lattice length	21.5984 cm
Water layer between assemblies	0.0734 cm
Baffle thickness	2.871 cm
Envelop inner radius	170 cm
Envelop thickness	5 cm
Neutron shield inner radius	181.15 cm
Neutron shield thickness	6.5 cm
Envelop and shield height	495.56 cm
Vessel inner radius	199.4 cm
Vessel thickness	20 cm
Vessel bottom inner sphere radius	200.6 cm
Vessel bottom thickness	15.5 cm
Concrete walls inner radius	269.4 cm
Vessel bottom to concrete floor distance	133.9 cm
Concrete floor thickness	50 cm
Metallic liner thickness	1 cm

The boron concentration in the water everywhere in the vessel is 1205 ppm by weight. The core is composed of 157 assemblies, whose dimensions are given in Table 1. The core is surrounded by a baffle of 2.871 cm thickness and a height corresponding to the fuel height. Around the baffle, the envelop (or the barrel) and the neutron shield are modeled as shown in Figure 3a. All dimensions of the structures inside and outside the vessel are given in Table 1. The water located between the baffle and the envelop is a mixture of borated water and steel since it takes into account the presence of steel reinforcements. Axially the assemblies modeling is simplified above the fissile zone and below it. 4 layers above and 5 layers below the fuel are defined identically over the whole core area up to the baffle. Heights and compositions of each layer are given in APPENDIX A.
All materials within the vessel were considered at the temperature of 559 K, using the TMP card of MCNP. The nuclear data used is ENDF-B\VII.1 at the temperature of 600K provided with MCNP. The molecular correction for thermal neutrons is taken into account for water in the whole geometry for the same temperature. (For 4 isotopes the nuclear data used was extracted from the JENDL-3.3 library : natural carbon, ^{14}N, ^{28}Si and ^{29}Si. In some rare cases these isotopes caused sampling problems for MCNP.)

2.2. Source term definition

In order to have comparable results, the neutron source is fixed. It is similar to a real neutron emission in the reactor model used in this study. The proposed distribution has an equal probability emission within an assembly, axially and radially, and the probability for each assembly is given in Table 2 imposing a 1/8 symmetry on the source term in the core. For compatibility reason with deterministic codes, the fission spectrum was converted into a histogram of the probability emission given in Table 3.

TABLE 2: Spatial probability of the neutron source emission in each assembly for an 1/8 core (mean value over the whole core is 1 for an assembly)

	H	G	F	E	D
8	1.085				
9	1.092	1.078			
10	1.073	1.088	1.081		
11	1.082	1.069	1.09	1.082	
12	1.059	1.068	1.056	1.064	0.9
13	1.056	1.036	0.985	0.936	0.711
14	1.015	1.052	0.977	0.652	
15	0.912	0.699			

TABLE 3: Biased and unbiased probability density for the neutron source energy

Probability	0	$5.33{\cdot}10^{-9}$	$1.18{\cdot}10^{-7}$	$1.22{\cdot}10^{-5}$	$2.48{\cdot}10^{-4}$	$5.84{\cdot}10^{-3}$	0.113
Biased probability	0	0	$1{\cdot}10^{-9}$	$1\cdot10^{-7}$	$1\cdot10^{-5}$	$1{\cdot}10^{-3}$	$4{\cdot}10^{-2}$
Upper energy [MeV]	$1\cdot10^{-9}$	$1\cdot10^{-5}$	$1\cdot10^{-4}$	$1\cdot10^{-3}$	$1\cdot10^{-2}$	$1\cdot10^{-1}$	0.5

Probability	0.159	0.43	0.29	$2.39{\cdot}10^{-3}$	$2.26{\cdot}10^{-4}$	$8.35{\cdot}10^{-6}$
Biased probability	0.2	0.55	0.7	0.4	$7{\cdot}10^{-2}$	$7{\cdot}10^{-3}$
Upper energy [MeV]	1	2	5	7	10	20

2.3. Detectors

Several detectors were considered in this study defined as spheres of 9 cm radius in the concrete of the reactor shield, shown in Figure 3. The detectors are located at 5 different positions referred to as B1, B3, C1, D1 and D3. The positions B1 and B3 are located at 70 cm below the midplane of the fissile zone, with an angle of 45° between the two detectors. Detector B1 is positioned in front of the assembly R8, following the nomenclature of Figure 2. The centers of spheres B1 and B3 are located radially 9.6 cm behind the inner radius concrete wall. The detector C1 is like B1 but shifted 4 meters below. Detector D3 is like C1 but shifted 178.6 cm below. Detector D1 is like D3 but shifted radially to the center of the geometry.

The detectors are volume track-length scores for the neutron flux at all energies and for the gamma flux at all energies. Thus, 10 detectors are proposed in this benchmark. Two comparisons will be performed, when the weight map is optimized for a single neutron detector at location B1 and another weight map optimized for all 10 responses simultaneously.

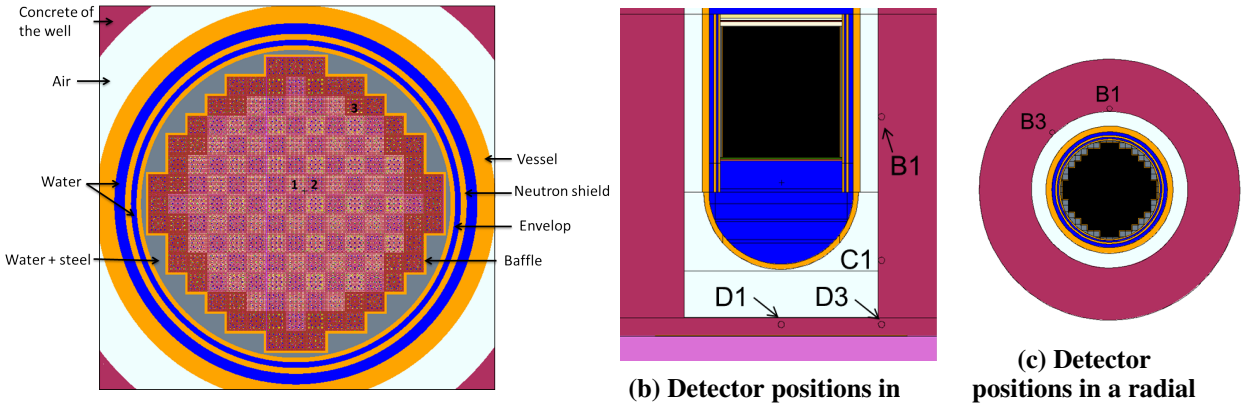

(a) Structures within the reactor shield, radial section in the MCNP model

(b) Detector positions in an axial section of the MCNP model

(c) Detector positions in a radial section of the MCNP model

FIGURE 3: MCNP geometry cross sections and detector positioning

2.4. Benchmark conditions

The aim in this benchmark is to compare weight maps produced by different methods, regarding the complexity and the effort needed by the user to produce them and the performance in terms of variance reduction. During the first step when the weight map is produced, no particular guidance is given in this benchmark. The user should in a very qualitative way give a judgment of the time spent during the first step and the level of experience required to employ the method. The second step is the evaluation of performance of the weight map with the Weight Window method in MCNP. For this step the comparison can be quantitative, so the authors used the same calculational machine (UBUNTU16, 20CPU, 32RAM) with the same parallelization and exactly the same simulation conditions : nps=$2{\cdot}10^8$, tasks=16. Depending on the method, source biasing can be used in addition to the weight map. If not specified otherwise, default weight window parameters ("WWP" card) were used for the final calculations.

3. Methods producing weight maps

Each method used to construct a weight map has its own peculiarities. Thus, the obtained weight maps may have different spatial meshes and different energy groups, that make them difficult to compare directly, but only by analyzing the detector responses and their statistics. The codes used in this study are presented below and the main characteristics of the weight window maps are summarized in Table 4. The simulation time over the iterations needed to obtain the proposed variance reduction parameters is given for each method. These calculations were performed on different computers, so the values are not directly comparable between the methods. Nevertheless, the order of magnitude should be comparable. The considered results for the final calculation

performed for each weight map are : the score, the statistical uncertainty and the figure of merit (FOM). The results for the 1-detector and the 10-detector problem will be given in section 4.

TABLE 4: Characteristics of the weight window maps produced by the methods

	WWG	DSA	ATTILA	ADVANTG
Spatial Mesh	Cylindrical user-defined 3060 mesh cells	Macrocell-based user-defined 37/38 * mesh cells	Cartesian 10^6 mesh cells based on triangular $4{\cdot}10^6$ mesh cells	Cartesian user defined $2{\cdot}10^6$ mesh cells
Energy groups	User-defined : 7 for neutrons and 6 for photons	Single detector : 1 group, multiple detector : same as WWG	Fixed : 8 for neutrons based on a solver using 47 group BUGLE-96	Fixed : 47 for neutrons, 20 for photons, BPLUS

3.1. Weight Window Generator

The Weight Window Generator (WWG), initially introduced to improve the exponential transform behavior [5],[10], is widely used today to provide an estimation of the adjoint flux based on a previous Monte Carlo simulation. The problem is subdivided into user-defined phase space cells in which the importance is estimated by the expected score generated by a unit weight particle entering the cell. The principal problem of this method is the statistical nature of the WWG [5], as was also encountered for this benchmark. Another limitation of this method, linked to the fact that the importance is estimated considering directly the score of a track (not a relative contribution to the final score for example) is that it can be applied to a single detector response. Of course the user can define the detector as a union of two detectors or more, but this can be done safely only for detectors of similar scores.
To produce an optimal importance map with the WWG, several approaches were tested. Due to the statistical nature of the method a rather coarse phase space mesh was chosen, as detailed in Table 4. Two energy group sets were tested : 1 group for neutrons and 1 for photons, and 7 groups for neutrons and 6 for photons. The improvement due to introduction of energy groups is about a factor 8 on the FOM. The use of source biasing on the energy spectrum of the emitted neutrons (described in Table 3) also improves the results, but the improvement of the FOM is not better than a factor 1.4. The results presented here consider a source biasing and a discretization in energy of the weight windows. To find an optimal set of parameters an iterative process is applied : the weight window parameters from the first simulation are used to improve the statistics of the second simulation, and so on. For each step, 1 to 5 $\cdot 10^8$ neutrons are simulated. When starting from an analog simulation around 7 iterations are needed to obtain the best parameter set : the iterations are stopped when no significant change in the score and the FOM is observed at the next iteration. At each step the weight windows are normalized by a factor chosen by the user in order to have the lower weight bound between 0.1 and 1 in the phase-space cells of the source where the main contributors come from. Thus, the source neutrons created with a weight of 1 will not be split nor be subjected to Russian Roulette. If source biasing is used the normalization should be adapted.
The total simulation time over the iterations needed to obtain the proposed variance reduction pa-

∗. 37 for the single detector case (B1 neutrons) and 38 for the 10 detector case (n and γ)

rameters was around 40000 CPU. In order to test whether the obtained importance map was the "best" for the considered phase space discretization and the number of simulated source particles (5 $\cdot 10^8$), the WWG was run using the weight window parameters produced by ADVANTG, that give the adjoint flux on a finer phase space discretization described in section 3.4. The weight window parameters produced by the WWG with the iterative process or when using a deterministic based importance map are very close. Thus, this test confirms that there is no need to make additional iterations with the WWG. This statement does not mean that no better weight window parameters can be obtained when changing the phase-space segmentation or increasing the number of simulating particles. The obtained weight window lower bounds for the neutron detector B1 are shown in Figure 4.

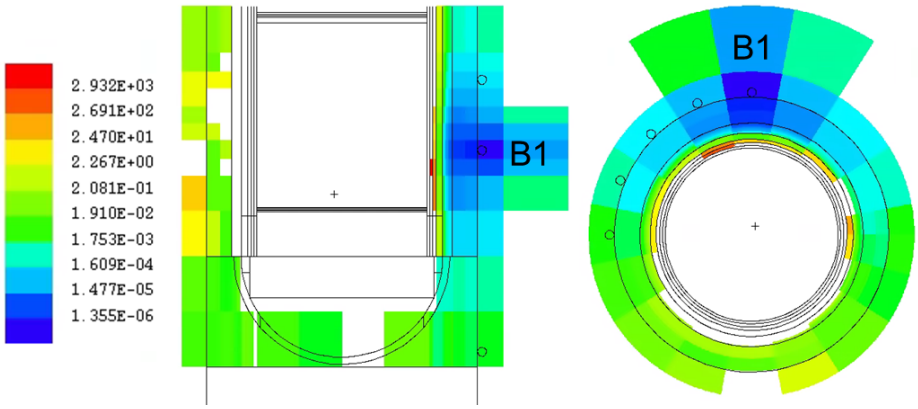

FIGURE 4: Weight window map for neutrons in the 6^{th} group (1eV-1keV) obtained with WWG

3.2. Direct Statistical Approach

Unlike the other methods studied in this paper, the DSA [6] method does not try to estimate the adjoint flux directly, but generates a set of parameters that maximize the FOM. Indeed the method [11] was originally developed to optimize population control through a rigorous statistical treatment of splitting and Russian Roulette. The advantage is the capability to estimate how the variance and the time, needed to compute the FOM, depend on the parameters. Coupled to an optimization function, it proposes a new set of parameters allowing to maximize the FOM. Additionally, it gives the user information on the estimated improvement of the FOM with the new parameter set. Using this method iteratively, allows to have a better variance and time function prediction, and thus to have an estimation of the convergence of the parameters. The constraints are a limited number of parameters and a greater calculational time (data storage and analysis or "bookkeeping") needed to generate and evaluate the variance and time functions.
Two approaches were used with the DSA. In the first approach only one detector was considered (neutrons in B1) and in the second one all 10 detectors were used for the optimization of the variance reduction parameters. For the single detector problem the same source biasing is used as described in Table 3 whilst with all 10 detectors, no source biasing was employed The spatial discretization used in this study is based on real geometrical cells. Since in contrast to the geometry cell definition the detector has an azimuthal dependence, the geometry was modified in order

to create smaller cells around the main streaming path of the particles where strong importance variations are expected. This step requires a rough guess by the user of the path of the particles.
For the first approach, the benchmark specifications suggest to start the iterative procedure with an analog calculation and $5{\cdot}10^8$ source particle histories. As the DSA deals in 2nd-moment quantities, it requires better statistics compared with classic 1st-moment approaches. The suggested number of source histories was not sufficient and we required double that number. 3 iteration steps were then needed to determine the optimal variance reduction parameters. For the final calculation the DSA cell variance reduction parameters were converted to weight window lower bounds and the following 'WWP' parameters were used : 2, 1.5, 1000, 1. The total simulation time over the iterations needed to obtain the proposed variance reduction parameters was 26656 CPU.
For the second approach, the geometry was adapted to the 5 detector locations. The iterative process was started from the optimum variance reduction parameters from the single detector case, expanded over the 7 neutron and 6 γ energy groups. 6 iterations were needed to obtain optimal variance reduction parameters for the 10 detectors simultaneously illustrated in Figure 5. The total simulation time over the iterations needed to obtain the proposed variance reduction parameters was 2403 CPU (although bearing in mind that the starting parameters were those obtained with the single detector). For both approaches, some manual adjustment was performed on the parameters by an experienced user *i.e.* some phase-space macro-cells were excluded from the variance reduction (weight window lower bound put to zero). Nevertheless, no significant impact of this adjustment is expected on the final results.

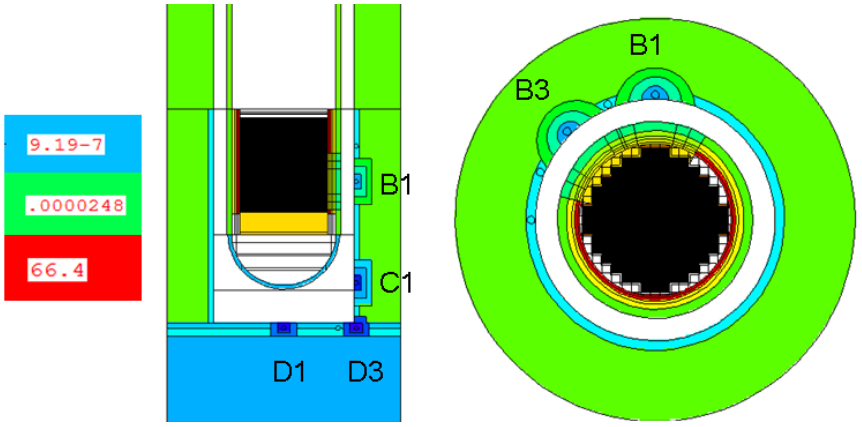

FIGURE 5: Weight window map for neutrons in the 6^{th} group (1eV-1keV) obtained with DSA for multiple detector problem (using the following 'WWP' parameters : 5, 3, 1000, 1)

3.3. ATTILA

The ATTILA tool allows to solve the Boltzmann equation with a three dimensional SN particle transport code with a multi-group energy discretization. It uses the discontinuous finite element spatial differencing techniques on an unstructured tetrahedral finite element mesh. Neutrons and photons can be treated in the same problem, using BUGLE-96 nuclear data. The geometry of the problem is based on a CAD model, that has to be created with another tool. The materials were provided directly to ATTILA using a simplified description of the assemblies, as for ADVANTG. The user interface allows to generate automatically the tetrahedral mesh, that is refined in the regions selected by the user. ATTILA4MC was used to produce the weight window parameters

for the MCNP calculation based on solving the adjoint problem for the detector. In the version available to the authors only the 1 detector problem † could be solved.
To evaluate the adjoint flux for 8 neutron groups (collapsed from the 47 neutron groups) ATTILA needed approximately $6{\cdot}10^6$ CPU. The calculation was rather long because the virtual memory available (128GB) was not optimal. The used solver parameters were : Sn order 32, Pn order 4 and Triangular Chebychev Legendre quadrature. The adjoint flux was then projected from the tetrahedral to the Cartesian mesh provided by the user for the weight windows.
The source definition was not integrated in the ATTILA tool, due to its complexity. Thus, no source biasing was calculated, but the energy source biasing from Table 3 was used. In Figure 6 far from the detector some ray effects are visible. Nevertheless no effect of these rays are expected on the result of the detector B1. The variation of the importance map produced by ATTILA is limited to 10^{10} in order to avoid some problems with MCNP [4]. For the one detector problem it is sufficient but it is questionable for the other detectors since the whole core may have the same importance for all neutron energy groups.

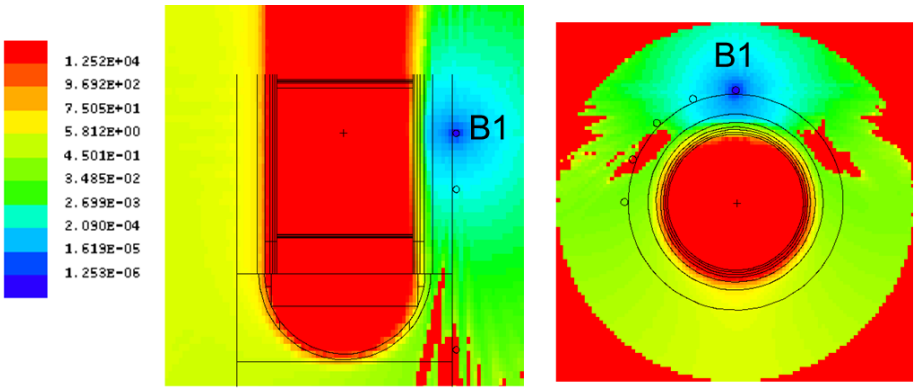

FIGURE 6: Weight window map for neutrons in the 2^{nd} group (5eV-1.58keV) obtained with ATTILA

3.4. ADVANTG

The ADVANTG tool is based on the SN transport code DENOVO using nuclear cross sections BPLUS [3]. The problem geometry and materials are calculated automatically based on the MCNP input file using a regular Cartesian spatial mesh. Several detectors for neutrons and photons can be specified using the FW-CADIS method. The authors had no previous experience with this tool. Nevertheless, using the calculation parameters close to default gave very satisfactory results. Relatively few verification tests were performed and certainly some optimization of the parameters may improve the results. The methodology used in FW-CADIS [12] is based on an adjoint calculation using an adjoint source that consists of weighted (with their respective scores) contributions from the 10 response functions to produce the weight window parameters. Since the results obtained for the 10 detectors gave also very good performance for the B1 detector, a separate single detector

†. As can be seen from Figure 6, the detector used in the ATTILA calculation is positioned higher than the one used by the other codes. This mistake should have no impact on the comparison, since the two detectors are positioned at +70cm/-70cm above/below the fissile mid-plane and the fluxes are the same for the two detectors.

analysis was not carried out.

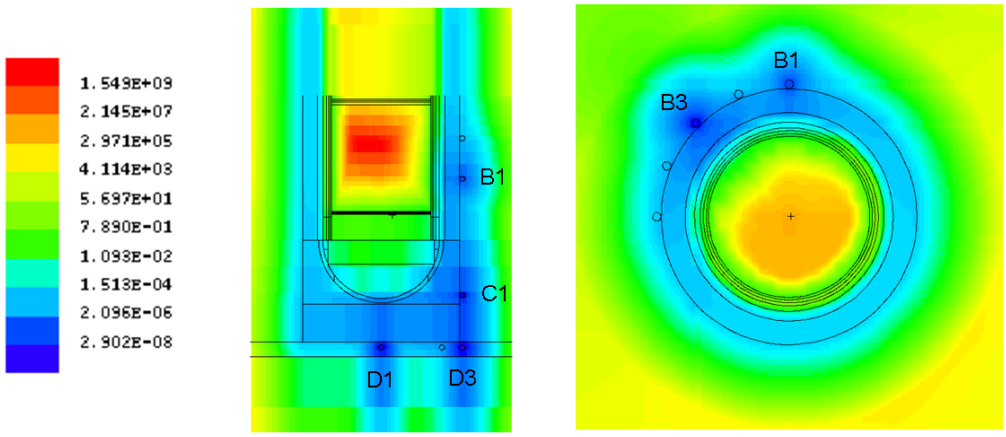

FIGURE 7: Weight window map for neutrons in the 10^{th} group (0.21-0.45 keV) obtained with ADVANTG (using the following 'WWP' parameters : 5, 3, 100, 0)

The geometry and materials provided to DENOVO were described through an MCNP input file, containing a simplified modeling of the assemblies. In the DENOVO solver, quadruple range product quadratures of order 10 with an angular scattering of the 3rd order, corresponding to ADVANTG default parameters, were used. The calculation took around 600 CPU. The weight window phase space mesh, as shown in Figure 7, was the same spatial Cartesian mesh and energy group structure as used by the solver. Since the spatial neutron source is cell-based and the ADVANTG version used in this study did not support multiple cell-based source definition, the CADIS methodology was not entirely applied. In the forward DENOVO calculation the source was positioned in the center of the reactor as a point source with energy distribution given in Table 3. The source energy biasing proposed by ADVANTG gave no better results than that in Table 3, whose results are presented in this paper.

4. Results

4.1. Single detector problem

The B1 detector responses for the different tools are compared in Table 5. All the detector responses agree with each other within 1 standard deviation, except ATTILA that is within 3 σ. Some additional test runs indicated that the statistics may be the reason for the flux underestimation for ATTILA response. The analog calculation presented in this table was calculated with $1.5{\cdot}10^{10}$ source particles. All the other calculations were performed with $5{\cdot}10^{8}$ source particles. All the results passed the 10 statistical tests implemented in MCNP. In some cases, for instance for WWG, the normalization of the weight window could lead to a higher FOM, but without passing all the 10 statistical tests. It was chosen to select the case in which all tests were good.
The acceleration, that can be read from FOM/FOM$_{anal}$, is very good up to a factor of $5 \cdot 10^5$. Its dispersion for all the methods does not exceed a factor 4, while ADVANTG proposes the highest FOM. When one compares DSA and ADVANTG weight window parameters, the ADVANTG mesh cells are much finer in the phase space ($2{\cdot}10^6$ x 47, stored in 1.4GB, compared to 37 x 1 cells),

TABLE 5: Results of the calculations using weight window parameters produced by different methods for the neutron flux detector in B1

	Analog	WWG	DSA	ATTILA	ADVANTG
$\phi[n/source\ particle]$	6.62E-07	6.42E-07	6.39E-07	6.13E-07	6.41E-07
$\sigma[\%]$	5.72	0.33	0.37	1.75	0.17
FOM $[min^{-1}]$	9.47E-04	24.47	35.88	15.42	52.53
FOM/FOM$_{anal}$	1	25836	37881	16280	55458

but yet the final FOMs are very close. However, the user experience and time required to generate the parameters are more important for the DSA tool. When considering at the FOM produced by ATTILA and ADVANTG, it had been expected to obtain similar results. The difference may be explained by the coarser energy groups in ATTILA code or to the non-optimal solver parameters used for this problem. The difference is not yet well understood and will be further investigated. The WWG gives also good results compared to the other codes.

4.2. Multi-detector problem

TABLE 6: Results of the calculations using weight windows produced by different methods regarding the neutron and photon total flux in 5 detectors

		neutrons			photons		
		Analog	DSA	ADVANTG	Analog	DSA	ADVANTG
B1	$\phi[n/source\ particle]$	6.63E-07	6.41E-7	6.41E-7	2.48E-7	2.27E-7	2.22E-7
	$\sigma[\%]$	5.72	0.27	0.17	9.4	1.33	0.62
	FOM $[min^{-1}]$	9.47E-4	5.9	52.53	3.51E-4	0.243	3.94
B3	$\phi[n/source\ particle]$	2.35E-7	2.46E-7	2.45E-7	9.62E-8	1.03E-7	9.81E-8
	$\sigma[\%]$	10.79	0.3	0.16	12.94	2.82	0.73
	FOM $[min^{-1}]$	2.66E-4	4.78	59.30	1.85E-4	5.41E-2	2.84
C1	$\phi[n/source\ particle]$	1.56E-8	1.51E-8	1.51E-8	1.06E-8	1.32E-8	1.19E-8
	$\sigma[\%]$	44.39	0.56	0.99	43.28	7.85	4.77
	FOM $[min^{-1}]$	1.57E-5	1.37	1.54	16.54E-6	6.98E-3	6.67E-2
D1	$\phi[n/source\ particle]$	8.44E-9	7.60E-9	7.55E-9	3.84E-9	5.96E-9	6.07E-9
	$\sigma[\%]$	44.11	0.36	0.85	49.52	1.79	4.94
	FOM $[min^{-1}]$	1.59E-5	3.32	2.10	12.64E-6	0.134	6.22E-3
D3	$\phi[n/source\ particle]$	1.36E-9	5.41E-9	5.37E-9	9.16E-10	3.97E-9	4.17E-9
	$\sigma[\%]$	92.99	1.03	0.74	69.17	0.87	4.57
	FOM $[min^{-1}]$	3.58E-6	0.405	2.77	6.48E-6	0.568	7.27E-3

Among the 4 methods tested, only ADVANTG and DSA allow a multi-detector problem solving. The results are given in Table 6. In general, the two methods provide a great acceleration from 100 up to a factor 10^6 on the FOM, depending on the position and particle type. (However note that the analog σ is so high for detectors C1, D1 and D3 that their respective FOM's are not very meaningful.) The FOM's obtained with ADVANTG are for many detectors greater than those with the DSA, especially for neutrons. Nevertheless, the photon response in detector C1 may be improved

for both methods. The overall average uncertainty is still low and very similar for both methods : 1.85% for ADVANTG, varying from 0.16% to 4.94%, and 1.72% for DSA, varying from 0.25% to 7.85%. For both methods the neutron responses have lower uncertainty than the photons. Since the photon history calculation time is much shorter than that of the neutron, as already suggested in [7], the photons could be additional split to improve the results for ADVANTG. Another lead is to refine the spatial mesh around the detectors to improve the photon responses for both methods.

5. CONCLUSIONS

The aim of this paper is to propose a calculation benchmark for methods that allow to construct weight window parameters for neutrons and photons to be transported with MCNP. Several methods were tested on a nuclear power reactor model, seeking neutron and photon responses outside the reactor core vessel. The comparison of tested methods (WWG, DSA, ADVANTG and ATTILA) gave similar performances for the 1-detector problem, whereas the amount of effort required by the user may be different, depending also on the user experience (*i.e.* having deterministic code background) or having access to a CAD model of the problem already. For the multi-detector problem, only two methods (ADVANTG and DSA) could be used, giving similar results and performances. The CADIS methodology could not be applied entirely for this problem due to technical issues linked to a spatially large source and a complex source definition. An improvement would be reached if the codes could support very complex source definitions. For instance, in this type of problems, the authors usually use a source definition based on the cells at pin level and axial segmentation, that passes through a source subroutine. In this case, the use of the CADIS method to produce the source biasing is not feasible today for technical reasons but may be an interesting feature.

REFERENCES

[1] *MCNP X-5 Monte Carlo Team, MCNP - A general Monte Carlo n-particle transport code, version 5*. Los Alamos National Laboratory (2005).

[2] J. Wagner and A. Haghighat. "Automated Variance Reduction of Monte Carlo Shielding Calculations Using the Discrete Ordinates Adjoint Function." *Nuclear Science and Engineering*, **volume 128**, pp. 186–208 (1998).

[3] S. W. Mosher, S. Johnson, A. M. Bevill, A. M. Ibrahim, C. Daily, T. M. Evans, J. Wagner, J. Johnson, and R. E. Grove. "ADVANTG - An Automated Variance Reduction Parameter Generator." *ORNL/TM-2013/416 Rev 1* (2015).

[4] T. A. Wareing, J. M. McGhee, and J. E. Morel. "ATTILA : A three-dimensional unstructured tetrahedral mesh discrete-ordinates transport code." In *Proceedings of the American Nuclear Society Annual Winter Meeting*, pp. 134–156. Washington, D.C. (1996).

[5] T. E. Booth and J. S. Hendricks. "Importance Estimation in Forward Monte Carlo Calculations." *Nuclear Technology - Fusion*, **volume 5**(1), pp. 90–100 (1984). URL https://doi.org/10.13182/FST84-A23082.

[6] K. W. Burn. "Optimizing Monte Carlo to Multiple Responses : The Direct Statistical Approach, 10 Years On." *Nuclear Technology*, **volume 175**, pp. 138–144 (2011).

[7] J. Hoogenboom and D. Legrady. "A critical review of the weight window generator in MCNP." In *Proceedings of The Monte Carlo Method : Versatility Unbounded In A Dynamic Computing World*, pp. 134–156. Chattanooga, Tennessee, (2005).

[8] H. Panek. "Qualification du système NEPTUNE - Ebauche d'une nouvelle chaîne de calcul basée sur les codes APOLLO et Tortise." *Note CEA-N-2092* (1979).

[9] M. Brovchenko, B. Dechenaux, K. W. Burn, P. Console Camprini, I. Duhamel, and A. Peron. "Neutron-gamma flux and dose calculations in a Pressurized Water Reactor (PWR)." *Proceedings of the ICRS-13, Paris, EPJ Web of Conferences*, **volume 153**, p. 05008 (2017).

[10] T. Booth. "Genesis of the Weight Window and the Weight Window Generator in MCNP -A Personal History." *Los Alamos Report LA-UR-06-5807* (2006).

[11] A. Dubi. "General statistical model for geometrical splitting in Monte Carlo - I and II." *Transport Theory and Statistical Physics*, **volume 14**, pp. 167–221 (1985).

[12] J. Wagner, D. E. Peplow, and S. W. Mosher. "FW-CADIS Method for Global and Regional Variance Reduction of Monte Carlo Radiation Transport Calculations." *Nuclear Science and Engineering*, **volume 176**, pp. 37–57 (2014).

APPENDIX A.

```
c material 2: fuel pin cladding Zr-4, density=4.32397e-2 at/bn/cm
m2 8016 3.06850E-04 40090 2.17274E-02 40091 4.73822E-03 40091 4.73822E-03  &
40092 7.24246E-03  40094 7.33959E-03  40096 1.18244E-03 26054 8.63012E-06  &
26056 1.35474E-04  26057 3.12870E-06  26058 4.16372E-07 24050 3.28108E-06  &
24052 6.32724E-05  24053 7.17459E-06  24054 1.78591E-06 50112 4.65212E-06  &
50114 3.16536E-06  50115 1.63064E-06  50116 6.97338E-05 50117 3.68333E-05  &
50118 1.16159E-04  50119 4.11976E-05  50120 1.56254E-04 50122 2.22055E-05  &
50124 2.77688E-05
c material 3: water w. 1205 ppm boron (19.9w%B10), density=7.5736e-2 at/bn/cm
m3 1001 5.04567E-02  8016 2.52283E-02  5010 1.00808E-05 5011 4.05763E-05
c material 5: water with boron + structure materials around the guide tube
c density=7.6040e-2  at/bn/cm
m5 1001 4.87578E-02  8016 2.43789E-02  5010 9.74133E-06  5011 3.92101E-05  &
26054 7.82898E-05  26056 1.22898E-03  26057 2.83826E-05 26058 3.77720E-06  &
24050 2.79517E-05  24052 5.39021E-04  24053 6.11206E-05 24054 1.52142E-05  &
28058 5.18394E-04  28060 1.99684E-04  28061 8.68015E-06 28062 2.76761E-05  &
28064 7.04829E-06  13027 2.24420E-05  41093 7.14577E-06 25055 4.32688E-05  &
42092 3.07529E-06  42094 1.92180E-06  42095 3.31057E-06 42096 3.47298E-06  &
42097 1.99051E-06  42098 5.03665E-06  42100 2.01341E-06 22046 1.35547E-06  &
22047 1.22239E-06  22048 1.21122E-05  22049 8.88863E-07 22050 8.51074E-07
c material 6: helium for instrumentation tube, density=9.55554e-4 at/bn/cm
m6 2004   9.55554E-04
c material 7: SS-316 intrumentation tube, density=8.4777e-2 at/bn/cm
m7 26054 3.28246E-03  26056 5.15277E-02 26057 1.19000E-03 26058 1.58367E-04 &
24050 6.74913E-04   24052 1.30150E-02  24053 1.47580E-03  24054 3.67358E-04 &
28058 6.88816E-03  28060 2.65331E-03  28061 1.15337E-04  28062 3.67746E-04  &
28064 9.36541E-05  25055 1.72947E-03 42092 1.82816E-04  42094 1.14244E-04   &
42096 2.06457E-04  42097 1.18329E-04 42098 2.99412E-04 42100 1.19690E-04   &
42095 1.96802E-04
c material 8: SS-304, density=8.42894e-2 at/bn/cm
m8  26054 3.25415E-03 26056 5.10832E-02 26057 1.17973E-03 26058 1.57001E-04 &
24050 7.85976E-04  24052 1.51568E-02 24053 1.71865E-03  24054 4.27810E-04   &
28058 6.00005E-03  28060 2.31121E-03  28061 1.00467E-04  28062 3.20332E-04  &
28064 8.15791E-05  25055 1.71246E-03
c material 9: poison, density=7.03475e-2 at/bn/cm
m9  8016 4.42534E-02 5010 1.41178E-03 5011 5.68258E-03 13027 2.00841E-03  &
14028 1.35898E-02  14029 6.90370E-04 14030 4.55629E-04 11023 1.36040E-03  &
19039 8.34745E-04  19040 1.04726E-07 19041 6.02414E-05
c material 10: water + Inconel 718 between ass., density=7.6038e-2 at/bn/cm
m10 1001 4.89223E-02 8016 2.44611E-02  5010 9.77420E-06 5011 3.93424E-05  &
26054 1.71050E-05  26056 2.68512E-04  26057 6.20111E-06 26058 8.25253E-07 &
24050 2.77955E-05  24052 5.36008E-04  24053 6.07790E-05 24054 1.51292E-05 &
28058 1.01042E-03  28060 3.89211E-04  28061 1.69187E-05 28062 5.39443E-05 &
```

```
28064 1.37380E-05  13027 5.87315E-05 41093 1.87008E-05  25055 1.44176E-05 &
42092 8.04817E-06  42094 5.02943E-06  42095 8.66391E-06 42096 9.08893E-06 &
42097 5.20924E-06  42098 1.31811E-05  42100 5.26918E-06 22046 3.54733E-06 &
22047 3.19905E-06  22048 3.16981E-05 22049 2.32619E-06  22050 2.22730E-06
c material 11: water + inconel between fuel pins, density=7.57903e-2 at/bn/cm
m11 1001 5.01800E-02  8016 2.50900E-02  5010 1.00255E-05 5011 4.03538E-05 &
26054 3.08464E-06  26056 4.84223E-05 26057 1.11828E-06  26058 1.48823E-07 &
24050 5.01252E-06  24052 9.66615E-05  24053 1.09606E-05 24054 2.72834E-06 &
28058 1.82215E-04  28060 7.01888E-05  28061 3.05106E-06 28062 9.72810E-06 &
28064 2.47746E-06  13027 1.05914E-05  41093 3.37241E-06 25055 2.60001E-06 &
42092 1.45137E-06  42094 9.06983E-07  42095 1.56241E-06 42096 1.63906E-06 &
42097 9.39410E-07  42098 2.37702E-06  42100 9.50220E-07 22046 6.39710E-07 &
22047 5.76902E-07  22048 5.71629E-06  22049 4.19495E-07  22050 4.01660E-07
c material 12: water between baffle & envelop density=7.6201e-2 at/bn/cm
m12 1001 4.77118E-02  8016 2.38559E-02  5010 9.53236E-06 5011 3.83689E-05 &
26054 1.77026E-04  26056 2.77893E-03 26057 6.41775E-05  26058 8.54085E-06 &
24050 4.27570E-05  24052 8.24527E-04  24053 9.34947E-05 24054 2.32728E-05 &
28058 3.26403E-04  28060 1.25730E-04  28061 5.46539E-06 28062 1.74261E-05 &
28064 4.43790E-06  25055 9.31578E-05
c material m14: AIR, density=5.3248e-05 at/bn/cm
m14 7014 4.1985E-05  8016 1.1263E-05
c material m15: lower part core h1, height=1.75cm density=6.2671e-2 at/bn/cm
m15  1001 2.94667E-02 8016 1.48577E-02  5010 5.88716E-06 5011 2.36966E-05 &
40090 8.80083E-03  40091 1.91925E-03 40092 2.93361E-03 40094 2.97295E-03  &
40096 4.78957E-04  26054 3.92914E-05  25055 1.88371E-05 26056 6.16790E-04 &
26057 1.42444E-05  26058 1.89567E-06  24050 9.97475E-06 24052 1.92353E-04 &
24053 2.18113E-05  24054 5.42930E-06  28058 6.60006E-05 28060 2.54233E-05 &
28061 1.10513E-06  28062 3.52365E-06  28064 8.97369E-07 50112 1.88438E-06 &
50114 1.28216E-06  50115 6.60504E-07  50116 2.82463E-05 50117 1.49196E-05 &
50118 4.70512E-05  50119 1.66874E-05  50120 6.32919E-05 50122 8.99452E-06 &
50124 1.12480E-05
c material m16: lower part core h2, height=2.30cm density= 7.4108e-2 at/bn/cm
m16 1001 4.72275E-02  8016 2.36300E-02  5010 9.43558E-06 5011 3.79794E-05 &
40090 1.15171E-03  40091 2.51161E-04  40092 3.83904E-04  40094 3.89053E-04 &
40096 6.26783E-05  26054 3.62531E-05  26056 5.69096E-04  26057 1.31429E-05  &
26058 1.74908E-06  24050 8.81965E-06  24052 1.70078E-04  24053 1.92855E-05 &
24054 4.80057E-06  28058 6.60006E-05  28060 2.54233E-05  28061 1.10513E-06 &
28062 3.52365E-06  28064 8.97369E-07  25055 1.88371E-05 50112 2.46597E-07   &
50114 1.67788E-07  50115 8.64362E-08 50116 3.69642E-06  50117 1.95244E-06  &
50118 6.15731E-06  50119 2.18378E-06  50120 8.28262E-06  50122 1.17706E-06 &
50124 1.47196E-06
c material m17: lower part core h3, height=1.93cm density= 8.2761e-2 at/bn/cm
m17 1001 9.01661E-03  8016 4.50830E-03  5010 1.80143E-06 5011 7.25098E-06 &
26054 2.67263E-03  26056 4.19546E-02  26057 9.68915E-04  26058 1.28945E-04 &
24050 6.45519E-04  24052 1.24482E-02  24053 1.41153E-03  24054 3.51359E-04  &
28058 4.92784E-03  28060 1.89820E-03  28061 8.25133E-05  28062 2.63088E-04 &
28064 6.70009E-05  25055 1.40644E-03
c material m18: lower part core h4, height=12.37cm density= 7.6269e-2 at/bn/cm
m18  1001 4.73132E-02  8016 2.36566E-02  5010 9.45272E-06 5011 3.80484E-05 &
26054 2.02734E-04  26056 3.18249E-03 26057 7.34975E-05  26058 9.78117E-06  &
24050 4.89664E-05  24052 9.44269E-04  24053 1.07072E-04  24054 2.66526E-05  &
28058 3.73803E-04  28060 1.43988E-04  28061 6.25908E-06 28062 1.99567E-05 &
28064 5.08238E-06  25055 1.06686E-04
c material m20 ; upper part core h6, height=11.42cm density=4.8469e-2 at/bn/cm
m20 1001 2.77714E-02 8016 1.39147E-02  5010 5.54845E-06 5011  2.23332E-05 &
40090 2.05787E-03  40091 4.48771E-04 40092 6.85956E-04  40094 6.95156E-04 &
40096 1.11993E-04  26054 9.25844E-05  26056 1.45338E-03 26057 3.35648E-05 &
26058 4.46686E-06  24050 2.24752E-05  24052 4.33413E-04  24053 4.91455E-05 &
24054 1.22334E-05  28058 1.69201E-04  28060 6.51761E-05  28061 2.83316E-06  &
```

```
28062 9.03335E-06  28064 2.30053E-06  25055 4.82914E-05 2004  3.12179E-04  &
50112 4.40619E-07  50114 2.99802E-07  50115 1.54444E-07 50116 6.60474E-06 &
50117 3.48861E-06  50118 1.10018E-05  50119 3.90197E-06  50120 1.47993E-05 &
50122 2.10316E-06  50124 2.63008E-06
c material m21 ; upper part core h7, height=3.37cm density=5.2379e-2 at/bn/cm
m21 1001 2.51375E-02  8016 1.25978E-02  5010 5.02223E-06 5011 2.02151E-05 &
40090 2.05787E-03  40091 4.48771E-04  40092 6.85956E-04 40094 6.95156E-04 &
40096 1.11993E-04  26054 1.44445E-04  26056 2.26748E-03 26057 5.23660E-05 &
26058 6.96895E-06  24050 1.06748E-04  24052 2.05853E-03 24053 2.33421E-04 &
24054 5.81035E-05  28058 3.23269E-03  28060 1.24523E-03 28061 5.41291E-05 &
28062 1.72587E-04  28064 4.39529E-05  13027 1.78068E-04 42092 2.44012E-05 &
42094 1.52487E-05  42095 2.62681E-05  42096 2.75567E-05 42097 1.57939E-05 &
42098 3.99638E-05 42100 1.59756E-05  22046 1.07552E-05  22047 9.69919E-06 &
22048 9.61054E-05  22049 7.05277E-06  22050 6.75293E-06 41093 5.66988E-05 &
25055 9.20041E-05  2004 2.73957E-04  50112 4.40619E-07  50114 2.99802E-07 &
50115 1.54444E-07  50116 6.60474E-06  50117 3.48861E-06 50118 1.10018E-05  &
50119 3.90197E-06  50120 1.47993E-05  50122 2.10316E-06 50124 2.63008E-06
c material m22 ; upper part core h8, height=1.82cm density=6.1660e-2 at/bn/cm
m22 1001 2.77714E-02  8016 1.40104E-02  5010 5.54845E-06 5011 2.23332E-05 &
40090 8.83123E-03  40091 1.92588E-03  40092 2.94374E-03 40094 2.98322E-03 &
40096 4.80611E-04  26054 9.56003E-05  26056 1.50072E-03 26057 3.46582E-05 &
26058 4.61237E-06  24050 2.35767E-05  24052 4.54653E-04 24053 5.15540E-05 &
24054 1.28329E-05  28058 1.69802E-04 28060 6.54072E-05  28061 2.84321E-06 &
28062 9.06539E-06 28064 2.30869E-06  25055 4.84626E-05 2004  1.42378E-05  &
50112 1.89089E-06 50114 1.28659E-06  50115 6.62787E-07 50116 2.83439E-05  &
50117 1.49712E-05 50118 4.72138E-05 50119 1.67451E-05  50120  6.35106E-05 &
50122  9.02560E-06  50124  1.12869E-05
c material m23 ; upper part core h9, height=4.56cm density=7.5511e-2 at/bn/cm
m23 1001 4.78582E-02  8016 2.39316E-02  5010 9.56159E-06 5011 3.84866E-05 &
40090 1.80362E-04  40091 3.93326E-05 40092 6.01208E-05  40094 6.09270E-05 &
40096 9.81563E-06  26054 1.27960E-04  26056 2.00869E-03 26057 4.63895E-05 &
26058 6.17359E-06  24050 3.09160E-05  24052 5.96185E-04 24053 6.76026E-05 &
24054 1.68277E-05  28058 2.35802E-04  28060 9.08306E-05 28061 3.94834E-06 &
28062 1.25890E-05  28064 3.20606E-06  25055 6.72997E-05 2004 3.72666E-06  &
50112 3.86181E-08  50114 2.62762E-08  50115 1.35362E-08 50116 5.78873E-07 &
50117 3.05760E-07  50118 9.64258E-07  50119 3.41989E-07 50120 1.29709E-06 &
50122 1.84332E-07  50124 2.30514E-07
c material m24 ; upper part core h10, height=11.49cm density=8.0242e-2 at/bn/cm
m24 1001 2.38761E-02  8016 1.19381E-02  5010 4.77021E-06 5011 1.92007E-05 &
26054 1.71429E-03  26056 2.69106E-02 26057 6.21484E-04  26058 8.27081E-05 &
24050 4.14051E-04  24052 7.98457E-03 24053 9.05386E-04  24054 2.25370E-04 &
28058 3.16083E-03  28060 1.21755E-03 28061 5.29259E-05  28062 1.68751E-04 &
28064 4.29759E-05 25055 9.02124E-04
c material 25 : concrete, density=2.39 g/cm3
m25 6000 1.9197057E-3 1001 4.521245E-03 1002 6.782885E-05 13027 2.840734E-04 &
20040 4.391428E-03 20042 2.930940E-05 20043  6.115563E-06 20044 9.467798E-05 &
20048 8.471188E-06  20046 1.812019E-07 14028 1.516251E-02 14029 7.698800E-04 &
14030 5.074993E-04 8016 1.103021E-02 8017 4.201481E-06
c material 27 : concrete + steel, density= 6.71030E-02 at/bn/cm
m27                 6000 3.22878E-03   1001 7.60435E-03   1002 1.14082E-04 &
13027 4.77787E-04  20040 7.38600E-03  20042 4.92959E-05  20043 1.02859E-05 &
20044 1.59240E-04  20048 1.42478E-05  20046 3.04766E-07  14028 2.55020E-02 &
14029 1.29487E-03  14030 8.53570E-04   8016 1.85519E-02   8017 7.06653E-06 &
26054 7.13906E-05  26056 1.12068E-03  26057 2.58813E-05  26058 3.44434E-06 &
24050 1.72430E-05  24052 3.32515E-04  24053 3.77043E-05  24054 9.38543E-06 &
28058 1.31631E-04  28060 5.07041E-05  28061 2.20408E-06  28062 7.02754E-06 &
28064 1.78971E-06  25055 3.75685E-05
```